Brief Communications

Homeostatic Interactions at the Front of Migration Control the Integrity and the Efficiency of a Migratory Glial Chain

Sara Berzsenyi, Arun Kumar, and Angela Giangrande

Institut de Génétique et de Biologie Moléculaire et Cellulaire, CNRS/INSERM/Université de Strasbourg, BP10142, 67404 Illkirch Cedex, CU de Strasbourg, France

In metazoans, cell migration often occurs in a collective manner: the cells move while physically and functionally connected to their neighbors. The coordinated and timely movement of the cells eventually ensures the proper organization of tissues, and deregulation in such a process contributes to the development of severe diseases. Thus, understanding the cellular mechanisms underlying coordinated cell movement is of great interest in basic and medical science.

The developing *Drosophila* wing provides an excellent model to follow the chain migration of glial cells *in vivo*. Cells at the tip of the glial collective have been shown to control the timely movement of the chain. In the present study, we show that while pioneers trigger chain migration, they cannot move as single cells. We also show that isolating cell clusters at the chain tip restores the formation of smaller migratory communities. Interestingly, the migratory efficiency of these *de novo* formed communities depends on the number of cells and progressively improves as the size of the cluster increases. Thus, homeostatic events at the migratory front control community integrity, efficiency, and coordination, emphasizing the importance of interactions and cell counting in fine-tuning collective processes.

Introduction

The correct pattern of complex tissues like the vertebrate nervous system arises from the coordinated migration of cells that are connected to each other (Marín et al., 2010). Defects in this collective process lead to neural diseases, and disruption of tissue cohesiveness may result in the mobilization of tumor cells (Friedl et al., 2004; Valiente and Marín, 2010). During the last decade, we have gained important insights on the molecular specification of leader versus follower cells at the tip of a migrating cohort (Ghabrial and Krasnow, 2006; Hellström et al., 2007). "Supracellular" molecular structures have also been recently shown to control migratory community integrity and coordination (Friedl and Gilmour, 2009). The cellular bases and the role of the homeostatic interactions occurring at the migratory front remain, however, poorly understood, due to the dynamic and complex nature of such interactions.

In the present study, we address this issue *in vivo*, in a system that allows tracing of collectively migrating cells. Using targeted ablation, we previously showed that four cells at the tip of a glial chain in the *Drosophila* wing act as pioneers (Aigouy et al., 2008). We here show that pioneers cannot move in isolation. Furthermore, upon ablation at different positions in the tip region, we have separated cell clusters of different sizes. These *de novo* formed communities display migratory behaviors that depend on their cell number. A four-cell cluster migrates less efficiently than a six-cell cluster, which migrates less efficiently than a ten-cell cluster, a migratory community that recapitulates the features of an intact chain. Moreover, the four-cell cluster tends to reestablish contact with the neighboring chain more efficiently than the six-cell cluster, whereas the ten-cell cluster moves as an independent collective.

Thus, bidirectional interactions and cell-counting mechanisms at the chain tip control the efficiency of migration and the integrity of the community, two main aspects of collective migration.

Received May 17, 2011; revised July 8, 2011; accepted Aug. 6, 2011.

Author contributions: S.B. and A.G. designed research; S.B. performed research; S.B., A.K., and A.G. analyzed data; S.B., A.K., and A.G. wrote the paper.

S.B. was supported by Association Française contre les Myopathies, and the work in the laboratory was supported by INSERM, CNRS, Université de Strasbourg, Hôpital de Strasbourg, Association pour la recherche sur le cancer, Institut National du Cancer, and Agence nationale de la recherche. We thank the Developmental Studies Hybridoma Bank and FlyBase for providing material and information. We thank J. P. Vincent for the *UAS-Apoliner* flies, C. Diebold, C. Delaporte, the fly and the imaging facility for excellent technical assistance, and all laboratory members, especially O. Komonyi, for comments on the manuscript.

Correspondence should be addressed to Angela Giangrande, Institut de Génétique et de Biologie Moléculaire et Cellulaire, CNRS/INSERM/UdS, BP10142, 67404 Illkirch Cedex, CU de Strasbourg, France. E-mail: angela@igbmc.fr.

DOI:10.1523/JNEUROSCI.2473-11.2011

 0270-6474/11/3113722-06$15.00/0

Materials and Methods

Dissection, time-lapse and immunolabeling were as described previously (Aigouy et al., 2004, 2008; Soustelle et al., 2008). Animals of either sex were analyzed (total $n = 79$ time-lapses: 18 controls; 17 early ablations, 8 late ablations; 9 single-cell, 10 four-cell, 11 six-cell, and 6 ten-cell clusters). To keep a predetermined number of cells isolated, we sometimes performed a second round of ablations because new glia emerged nearby the cluster.

The *UAS-Apoliner* strain was from J. P. Vincent (MRC, London, UK). Antibodies were m-anti-22c10 (Developmental Studies Hybridoma Bank, 1:1000) and Cy3-anti-mouse (Jackson Laboratory, 1:500). Images and movies were processed using ImageJ (NIH). Statistical analysis was done by Student's *t* test; bars indicate SEM. For semiquantitative analyses, distances were calculated manually and then transformed into micrometers upon considering the used magnification.

Results

Dynamics of glial chain migration

The L1 sensory nerve of the developing *Drosophila* wing is ensheathed upon directional migration of a glial chain (Gian-

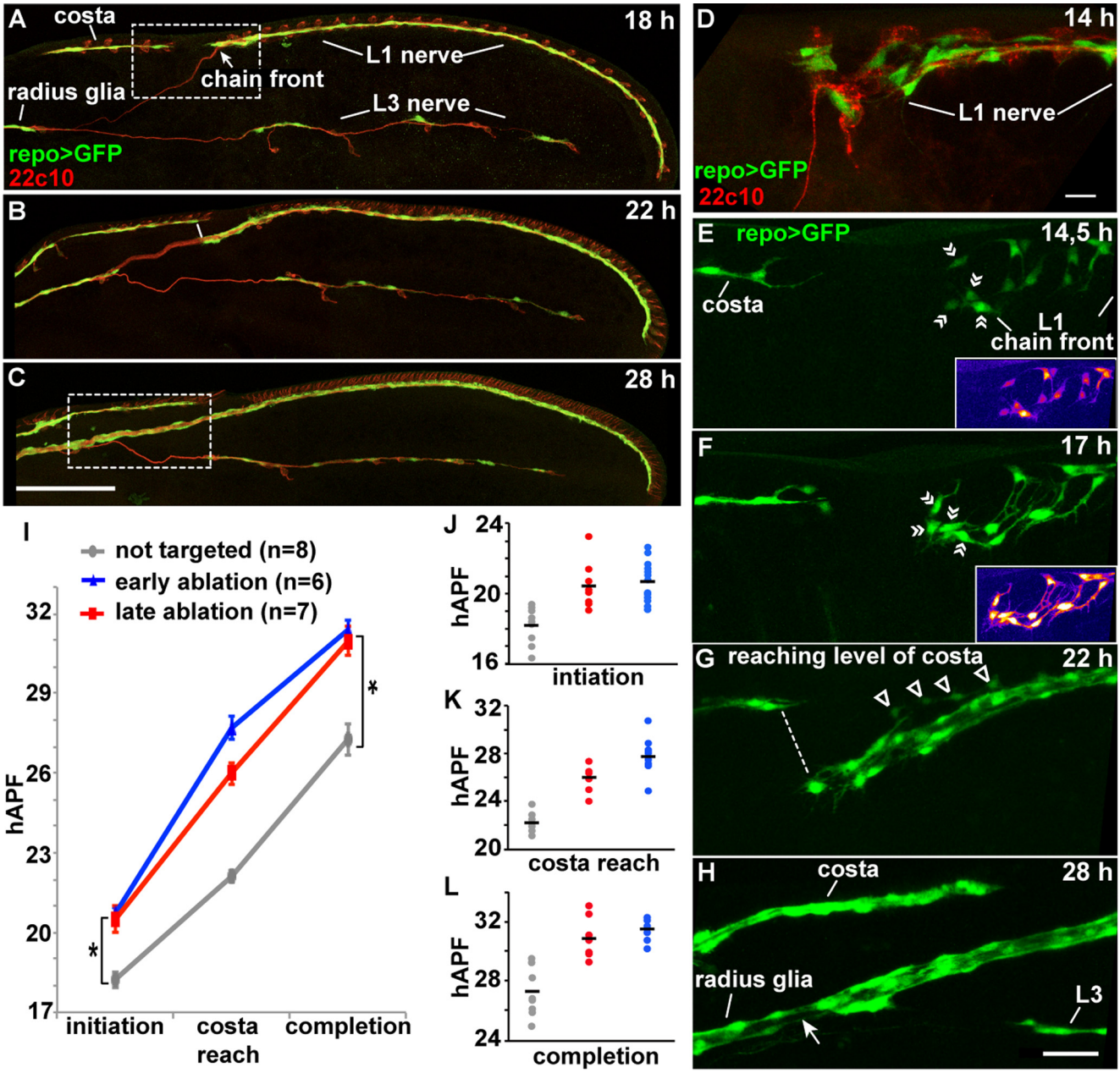

M	Initiation of migration (hAPF)				Reaching level of costa (hAPF)				Completion of migration (hAPF)			
	n	Average	Earliest	Latest	n	Average	Earliest	Latest	n	Average	Earliest	Latest
Control	10	18,2	16,4	19,5	10	22,1	21,1	23,7	8	27,2	25,0	29,6
Early ablation	17	20,7	19,1	22,7	11	27,7	24,8	30,7	6	31,4	30,8	32,3
Late ablation	8	20,5	19,1	23,3	8	26,0	23,9	27,3	7	31,0	29,4	33,1

Figure 1. Glial chain migration in a control wing and upon early/late ablation. ***A–D***, Immunolabeling showing wing glia (green) and neurons (anti-22c10, red) at different stages: onset of migration (***A***), reaching level of the costa (***B***), completion of migration (***C***), 14 hAPF (***D***). In all panels, proximal is to the left, anterior to the top. ***E–H***, In this and in following figures, snapshots show projections from time-lapses on *repo>GFP* wings. ***E–H*** correspond to the regions outlined in ***A*** and ***C***, respectively. ***E***, Before migration, glia show simple morphology and low GFP level (color-coded inset). ***F***, By 17 hAPF, GFP intensity is higher (inset) and cells extend filopodia. The four double arrowheads (***E***,***F***) indicate the position of the ablated cells. ***G***, By 22 hAPF, the migration front reaches the level of the costa. Open arrowheads show new glia appearing on the margin. ***H***, The glial chain completes migration (arrow), joining radius glia. ***I***, Graph representing migration efficiency in control wings and in wings in which the first four cells were ablated early or late (*$p < 0{,}05$, n = wing number). ***J–L*** show the raw data: ***J*** refers to migration initiation, ***K*** to reaching level of costa, and ***L*** to migration completion. The *x*-axis shows three experimental conditions: controls (gray circles), late-ablated wings (red circles), and early-ablated wings (blue circles). The *y*-axis indicates stages as hAPF. Each circle represents one sample; horizontal bars, average values. ***M***, Ablation data summary. The first column indicates the experimental conditions, the second, the third and the fourth columns indicate the stage of achievement (hAPF) of migration initiation, reaching the level of costa and completion. For each column, from left to right: wing number, average, earliest and latest stages. Bars: ***A–C***, 100 μm; ***D***, 10 μm; ***E–H***, 30 μm.

grande, 1994; Aigouy et al., 2004, 2008). During this period, the two wing epithelial blades are widely separated at the position of the L1 vein, creating a large cavity in which the nerve and the glia move (Fristrom et al., 1993). First the neurons send their axons proximally toward the CNS, then glia migrate along the axonal bundle and cover it (Fig. 1*A–C*,*E–H*). By 17–18 h after pupa formation (hAPF), glial cells start moving proximally along the nerve as shown by their soma translocation (Fig. 1*A*,*F*), and by 22 hAPF the chain front reaches the level of the nerve on the costal vein (Fig. 1*B*,*G*). The glial collective completes migration by 26–29 hAPF, upon joining the glia on the proximally located radial nerve (Fig. 1*C*,*H*).

Cells at the migration front display a network of exploratory filopodia and are indispensable for the proper timing of chain migration, since elimination of the first four cells at migration onset (17–18 hAPF) induces severe delay in glial coverage of the axonal bundle (Aigouy et al., 2008). Despite these dynamic features, pioneer cells are not observed in isolation; that is, they do not migrate independently from the collective. To address the issue of collective integrity, we decided to separate a tip cell from the chain and asked whether it has the potential to move in isolation. Unfortunately, at migration onset, the chain tip displays a complex organization (Aigouy et al., 2004, 2008), making it difficult to isolate cells. We therefore asked whether ablations could be performed at early stages, when tip cells may have a simpler organization. We could visualize glia as early as 14.5 hAPF, using *UAS-GFP;repogal4* (*repo > GFP*) transgenic flies that express nuclear and cytoplasmic GFP in all wing glia. At this stage, tip glia are located close to the neuronal somata and show simple morphology (few filopodia, low GFP intensity), and individual cells can be identified since they are arranged in a looser manner than at later stages (Fig. 1*D*). Between 14.5 and 17 hAPF, glia develop filopodia and accumulate GFP; limited, passive migration may be observed (Fig. 1*E*,*F*), mostly due to morphogenetic changes (wing extension and growth) occurring in this period. Because this initial modest shift is mostly passive, we focused on the active glial migration occurring after 17 hAPF.

Upon eliminating the first four cells at 14.5 hAPF, we found that early ablations affect chain migration like late ablations (18 hAPF) do. To define the overall migration efficiency, we performed very long confocal time-lapses and calculated the percentage of wings showing glia at a given position. We identified three steps: initiation (somata leaving the initial position), maintenance (reaching the level of costa), and completion of migration (reaching glia on the radius) (Fig. 1*A–C*,*I–M*). The delay in migration was similar between early and late ablations. In both cases, wings showed an initial delay of 2 h in average and chains kept migrating at a slower pace compared with control chains (average 4 h delay by migration completion) (Fig. 1*E–M*). The relatively small variability among the different samples shows the robustness of the migratory behavior at each step.

In sum, the pioneer activity is already detected by 14.5 hAPF, making it possible to analyze tip cell behavior upon early ablations.

Migration of individual pioneer cells requires contact to the collective

To determine the nature and role of the homeostatic interactions at the migratory front, we separated the first cell from the rest of the chain. We produced a gap upon targeted ablation and followed the migratory phenotype of the isolated cell as above. We used the *repo > GFP* ($n = 4$) or the *UAS-Apoliner;repogal4* (*repo > Apo-GFP*) transgenic line ($n = 5$), to score for apoptotic pathway activation. In *repo > Apo-GFP* flies, the glial membrane-tethered GFP localizes to the nucleus upon caspase activation (Bardet et al., 2008). Upon ablation of neighboring cells, the isolated cell did not emit the filopodia network typical of a pioneer and was eventually reached by the chain (Fig. 2*A–E*). In three cases, the isolated cell assumed rounded morphology and eventually underwent blebbing several hours after targeting (Fig. 2*A–E*). This suggests that the cell isolated from the chain entered the apoptotic pathway and hence could not migrate. In six cases, however, the isolated cell did not die and yet failed to migrate, subsequently getting incorporated into the slowly moving chain (Fig. 2*F–J*). The defective migration of apoptotic and non-apoptotic isolated cells suggests that connectivity controls both survival and cell movement. An experimental asset in which we were able to not completely separate the first cell confirmed this: the cell still in contact with neighbors distal to the gap was rapidly joined by the chain and recovered the migratory phenotype ($n = 2$) (Fig. 2*K–N*). The chain then completed migration with a delay comparable to the first four-cell ablated glial chain (Figs. 1*I–M*, 3*P*).

Thus, pioneer cells are controlled by the migratory community.

The size of the cluster determines its migratory efficiency

As tip cells cannot move in isolation, we asked whether separating a cluster of tip cells from the chain had a distinct effect and ablated cells behind the first four pioneer glia (Figs. 3*A–E*, 4*A–F*).

The isolated four-cell cluster did not initiate migration on time (Fig. 3*A–E*,*P–S*). Just after ablation, it exhibited a rather

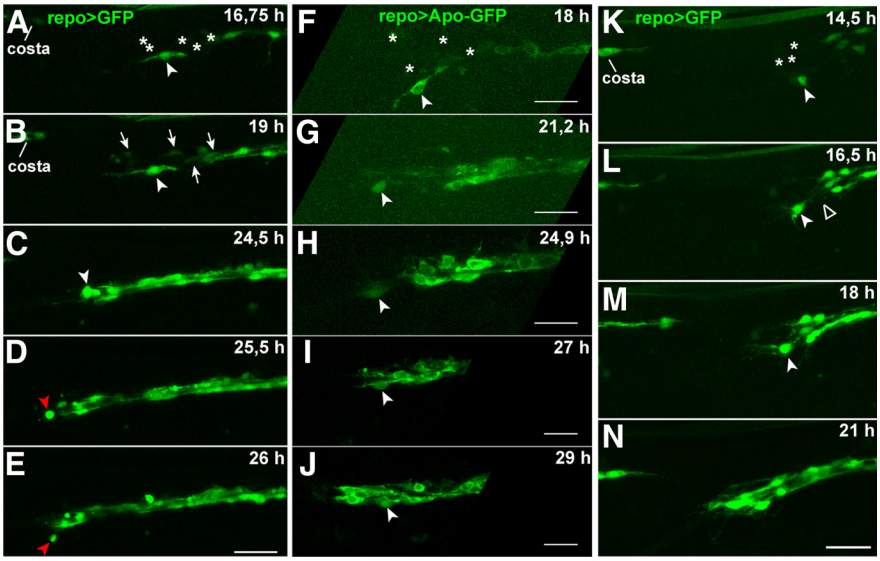

Figure 2. Single cell behavior upon isolation. The first cell is isolated by ablating cells behind it (asterisks in ***A***, ***F***, ***K***); genotypes are indicated. ***B***, Arrows indicate the UV-targeted, dying, cells. Several hours after isolation, the left-alone cell (white arrowhead) shows rounded morphology (***C***), then undergoes blebbing (red arrowheads in ***D***, ***E***). In ***F–N***, the isolated cell eventually reintegrates the chain, despite initial caspase activation (nuclear GFP) (***G–I***). ***L***, Empty arrowhead shows that the gap between the isolated cell and the chain is rapidly filled in this case and the joined cell resumes migrating. Bars: ***A–E***, ***K–N***, 30 μm; ***F–J***, 20 μm.

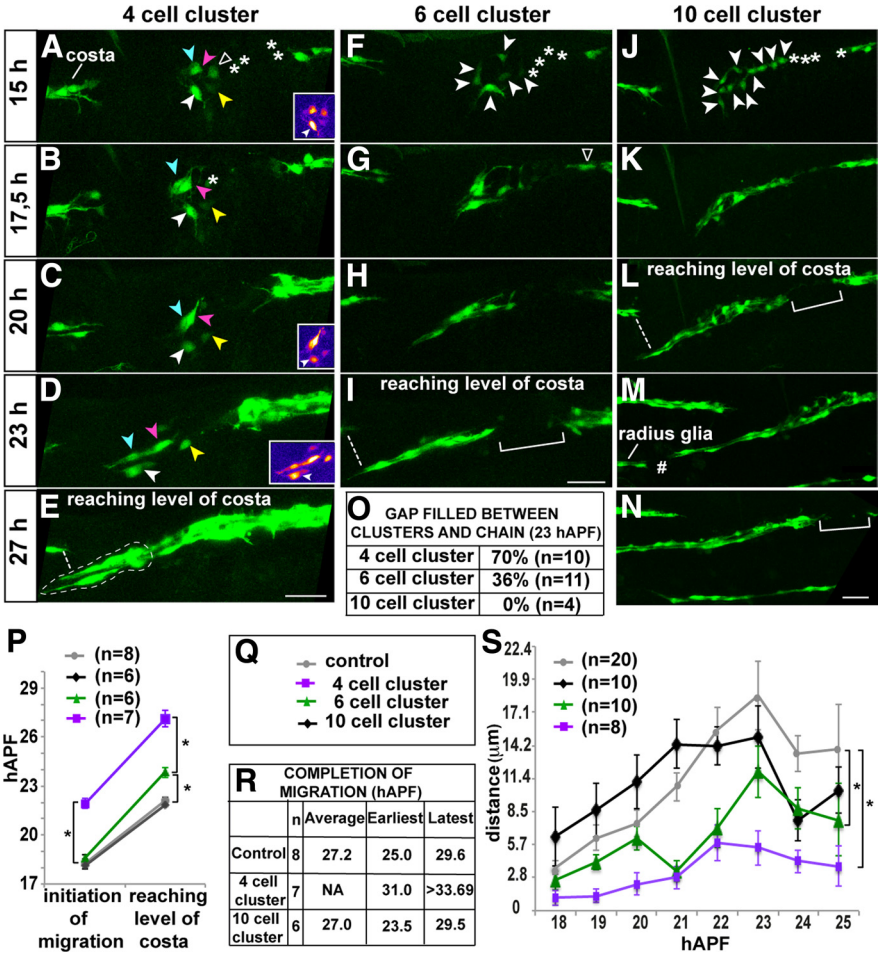

Figure 3. Migration efficiency upon isolating cell clusters of different sizes. Cell clusters are isolated upon UV-targeting (asterisks). ***A–E***, Four pioneer isolation (colored arrowheads). The cyan $^{+}$/magenta $^{+}$ cells (arrowheads) were initially identified as one cell; however, as it became obvious that they were two, the cell indicated by the open arrowhead was eliminated (asterisk in ***B***). The remaining four cells start migrating at ~22 hAPF and reach the costa by 27 hAPF (***E***) (see dashed line). GFP intensity initially decreases in one cell (white arrowhead, color-coded insets). GFP intensity and migration efficiency progressively recover (***D***, ***E***). ***F–I***, Six-cell cluster (F, arrowheads). To keep the cluster separated from the rest of the chain, additional ablation was performed (open arrowhead in ***G***). The gap between the separated group and the chain persists until 23 hAPF (bracket), when the cluster has reached the costa. ***J–N***, The ten-cell cluster (arrowheads) starts migrating and reaches the costa by 20 hAPF, as control chains. Note in ***K*** that a targeted cell still bridges the gap before disappearing at a later stage (***L***). ***M***, The cluster has almost completed migration by 23 hAPF (#) and by 27 hAPF is still separated from the distal chain (bracket in ***N***). ***O***, Percentage of wings in which the isolated clusters and the distal chains have reestablished contact by 23 hAPF. ***P***, ***Q***, Graph representing migration efficiency in control chains and in isolated clusters. Symbols as in Figure 1*I*. ***R***, Ablation data summary. For the four-cell clusters, migration was not always complete by the end of the time-lapse; therefore, the average time was not assessed (NA). ***Q***, ***S***, Graph showing the distance (μm, *y*-axis) covered each hour (hAPF, *x*-axis) by the soma of the proximal-most cell in control chains and in isolated clusters. Each point represents the average value, bars represent SEM. Bars, 30 μm.

simple morphology and the cell somata were not aligned along the axons. In some cases, the GFP intensity decreased in cells of the cluster (Fig. 3*A–C*, white arrowhead), suggesting that their overall health was affected; however, they subsequently resumed projecting cellular processes, aligning along the nerve, and recovered GFP expression. The cluster slowly resumed migration and was joined by the rest of the chain (Figs. 3*A–E*,*O*, 4*C*,*D*). The reconstituted chain completed migration with a delay as above (Figs. 1*I–M*, 3*P–S*). Thus, the four-cell cluster can migrate, albeit inefficiently.

The different behavior of the isolated first cell versus the four-cell cluster prompted us to ask whether the size of the cellular unit influences its functionality. We increased the number of cells in the isolated cluster and separated six to seven cells from the rest of the chain (Figs. 3*F–I*, 4*G–K*). Strikingly, the glia of the isolated group started to extend filopodia at the proper time before migration and accumulated the GFP as in control wings. The six-cell cluster started migrating on time compared with control chains and kept moving proximally while disconnected from the chain (Fig. 3*F–I*,*P–S*). Despite the obvious gap between the group of cells and the followers, the six-cell clusters formed a new chain and moved proximally (Fig. 3*H*,*I*), reaching the level of the costa later than control chains but earlier than the four-cell clusters (Fig. 3*I*,*P*,*S*). Eventually joined by the cells distal to the gap, the reconstituted glial chain reached the radius glia, albeit delayed compared with control chains (data not shown). In one-third of the cases, the six-cell clusters rapidly reestablished contact with the chain (vs two-thirds for the four-cell clusters) (Figs. 3*O*, 4*I*). Interestingly, disconnected and reconnected six-cell clusters reached the level of the costa with a similar delay (compare Figs. 3*I*, 4*J*) and both seemed more prone to migrate as a new chain than four-cell clusters (compare Figs. 3*I*, 4*K*; 3*D*, 4*D*).

Finally, isolated ten-cell clusters at the chain front moved as intact, control chains: they started migrating, reached the level of the costa, and finished migration as not-targeted glial collectives (or even before), even though they stayed disconnected (Figs. 3*J–S*, 4*L–Q*).

To evaluate migration efficiency in a semi-quantitative manner, we tried photoactivable-GFP transgenic lines (Murray and Saint, 2007) to follow the dynamics of individual cells over several hours. While this technique allowed us to trace small, epithelial cells, the signal/background ratio is too low for large and dynamic cells such as glia (S. Berzsenyi, unpublished observation). We therefore used conventional GFP lines and determined the average distance covered each hour by the soma of the proximal-most cell. This parameter provides the net cellular movement and is not affected by the fast changes and the variability of cytoplasmic protrusions. In control animals, cells initially migrated slowly, at the time of highly exploratory behavior. The speed of migration progressively and significantly increased until 23 hAPF and then slightly slowed down (Fig. 3*S*; data not shown). A similar profile was observed in the ten-cell clusters. Interestingly, the migration of the four-cell clusters was significantly slower at each time point and that of the six-cell clusters, initiated as the controls, slowed down precociously and subsequently recovered normal speed (Fig. 3*S*).

Thus, the ten-cell cluster shows migratory features that recapitulate those of a control chain; the four-cell clusters perform poorly in migration and tend to stay with the rest of the chain; the six-cell clusters behave in an intermediate manner.

Migratory behaviors around the gap reveal homeostatic interactions at the chain tip

The ablations behind the clusters allowed us to analyze the behavior of cells proximal and distal to the gap, shedding new light onto the collective migratory process.

One explanation for chain directionality is that contact inhibition enforces the proximal migration of tip cells. We have indeed shown that ablation in the middle of a migratory community releases contact inhibition, leading cells proximal to the gap to move backwards (Aigouy et al., 2004). If the same were true at the chain tip as well, inhibition would be lost when groups are isolated from the rest of the chain, accounting for the poor performance of small clusters in proximal migration. Regardless of the size of the restored community, however, the cells of the clusters do not migrate toward the gap (Figs. 3, 4). It is unlikely that the presence of cell debris and/or hemocytes prevents backward migration because we did see distal cells subsequently filling the gap (Figs. 3*A–E*, 4*B–F*). These data strongly suggest that cells at the chain tip actively move in a directional manner.

Interestingly, the cells distal to the gap did not become pioneers: they did not show the highly dynamic filopodia network of such cells and did not migrate as the tip cells of control chains or ten-cell clusters (Fig. 4*A*,*G*,*L*). Indeed, semiquantitative analyses showed that their migratory speed resembles that of the four-cell clusters (Fig. 4*A*). After the first hours, the distal chain migrated slightly more efficiently upon a four-cell than upon a six- or ten-cell cluster isolation (white arrows in Fig. 4*B–D*,*H–K*,*M–P*). This is likely explained by the fact that cells at each side of the gap slowly tried and reestablished physical contact, a process that was more successful when the cluster was small and not too motile (in some ten-cell cluster samples, the gap persisted until completion of migration; Figs. 3*N*,*O*, 4*P*).

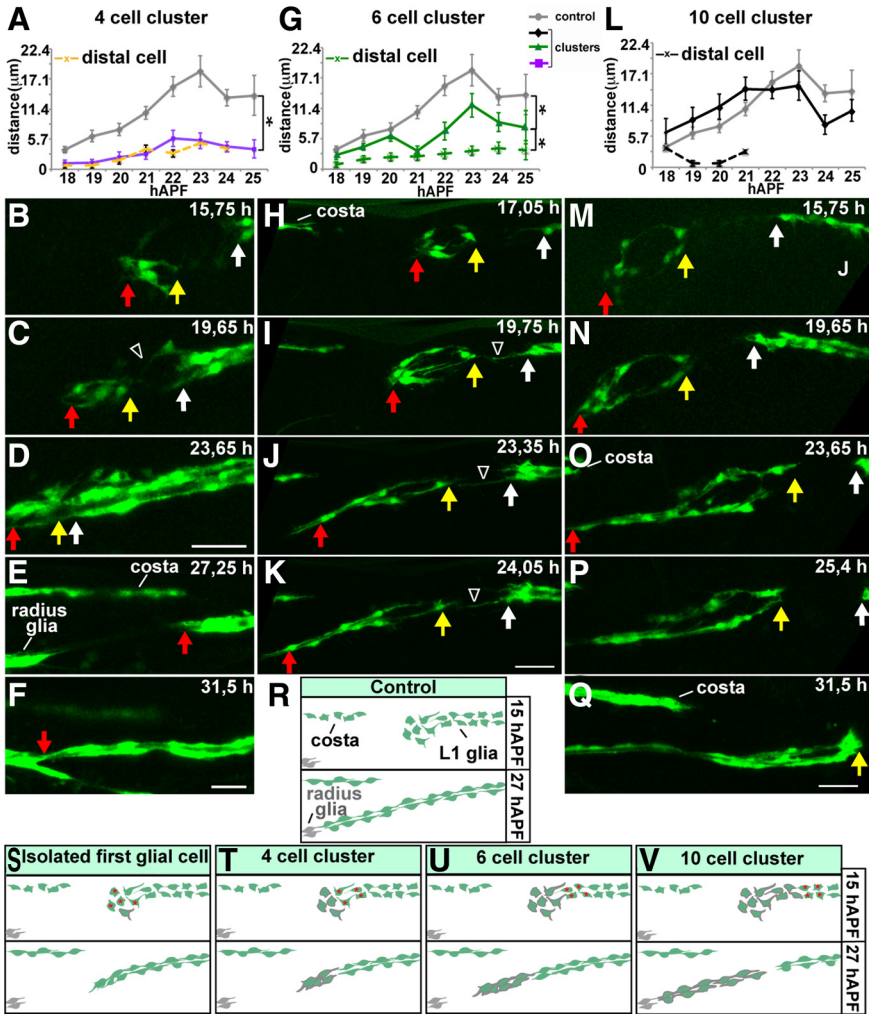

Figure 4. Migration dynamics in the gap region upon isolating clusters of different sizes. ***A***, ***G***, ***L***, Semiquantitative analysis as above showing the migratory behavior of clusters and cells distal to the gap. Distal cells in ***L*** could only be followed for a few hours, after which the stage was shifted to trace the rapidly moving cluster. ***B–F***, ***H–K***, ***M–Q***, Red and yellow arrows indicate proximal and distal cluster edges, respectively, and the white arrow, the proximal edge of the chain. Empty arrowheads indicate filopodia reestablishing connection. The relative positions of the arrows reveal the cell behavior in the gap region in four (***A–F***)-, six (***G–K***)-, and ten (***L–Q***)-cell clusters: in the first two cases, the gap is filled by 23 hAPF, whereas in the ten-cell cluster it persists until late (yellow arrow in ***M–Q***). This cluster moves more efficiently than the four- and the six-cell clusters, the XY microscope stage was therefore moved twice and once, respectively (check the costa reference point). Chain migration is indicated by white arrows in ***B–D***, ***H–K***, and ***M–P***. ***H–K*** show an extreme example of contact reestablishment: the proximal-most cells of the cluster send extensions backwards, seeking for contact with the chain. Similarly, a cell in the chain sends a long extension proximally. Strikingly, a cell in the cluster lags behind the others and bridges the gap between the cluster and the chain. ***R–V***, Schematic summary. Gray cells are radius glia, red asterisks indicate the UV-targeted cells, and green cells outlined in gray show the isolated one (***S***), four (***T***), six (***U***), and ten (***V***) cell(s). Scale bars, 30 μm.

Together, these data suggest that the isolated clusters do not move in response to contact inhibition and that the homeostatic interactions that finely tune the efficiency/integrity of the collective depend on the size of the cluster.

Discussion

A pioneer cell cannot move in isolation

Collective migration is a complex phenomenon in which cells constantly and actively interact with each other. In the present study, we have explored the role of specific cell interactions in the glial chain of the developing *Drosophila* wing. We show that the pioneer cells belong to a community and that they are not able to switch from collective to individual migratory behavior. Interestingly, this kind of transition has been observed in pathological conditions such as with primary melanoma explants *in vitro* (Hegerfeldt et al., 2002) and breast cancer cells *in vivo* (Giampieri et al., 2009). Also, a recent study has revealed the behavior of single mesendoderm cells of a zebrafish embryo in which a transplanted cell is able to migrate directionally isolated from its collective (Arboleda-Estudillo et al., 2010). Our data strongly suggest that collective migration adopts different strategies depending on the context: tumor cell plasticity is likely due to the metastatic nature (Friedl et al., 2004) and mesendodermal cells may constitute a quite homogeneous population, whereas glia at the tip are clearly morphologically and functionally distinct from those within the chain. This shows the importance of analyzing different models *in vivo*.

Homeostatic interactions at the tip of the migrating chain: sensing number?

Our data show that a cluster of tip cells is able to move directionally and that its migratory efficiency improves with the size of the cluster (Fig. 4*R–V*). The poor migratory efficiency of the small clusters might be an indirect consequence of pioneer fate changes, due to lack of contact with follower cells. If that were the case, however, the behavior of the four- and six-cell clusters should be similar. Indeed, we previously showed that the pioneer potential fades as the distance from the chain tip increases, the fifth and the sixth cells still contributing to it in a mild manner (Aigouy et al., 2008). The progressive improvement of the migratory features according to the cluster size rather leads us to propose that quantitative mechanisms are at work at the chain tip; that is, signaling pathways are reinforced/amplified by the increasing number of cells. We propose that cell-counting mechanisms provide robustness in complex behaviors, like the homeostatic interactions sensing cell density that allow microorganisms to make collective decisions (Boyen et al., 2009).

Several molecular mechanisms may control the observed behaviors. For their known role in migration or axonal guidance, potential pathways are those of RTK receptors and ligands, netrins and molecules controlling the extracellular matrix. Indeed, tip cells may not leave the chain because they must be provided enough trophic factors for their functioning. Also, small, isolated clusters may be unable to interpret shallow gradients of guidance cues that require integration across a tissue's length. Furthermore, the size of the cluster may be important to ensure directionality in dense environments, such as when cells migrate through the extracellular matrix. The identification of a collective mechanism at the chain tip sets the basis for studying the molecular nature of the "community effect," ensuring that cells belonging to one collective stay together and migrate efficiently.

It is now accepted that collective migration at suboptimal conditions may lead to diseases as severe as mental retardation and epilepsy (Valiente and Marín, 2010). Collective behaviors require the integration of complex pathways, and eliminating one of them does not necessarily produce clear-cut phenotypes, often hampering the use of genetic analyses. Our work shows that eliminating specific cells allow the analysis of subtle but scorable phenotypes. A current challenge is to provide computational models for collective migration (Vargas and Zaman, 2011); however, the value and significance of such models heavily relies on our knowledge of this complex and dynamic process. In the future, it will be of great interest to incorporate parameters that take into account the homeostatic cell interactions of the kind we have described, to faithfully simulate collective migration.

Notes

Supplemental material for this article is available at ftp://ftp-igbmc.u-strasbg.fr/pub/angela/SARAMOVIES_JNS.zip. Time-lapses related to data shown in this article. This material has not been peer reviewed.

References

Aigouy B, Van de Bor V, Boeglin M, Giangrande A (2004) Time-lapse and cell ablation reveal the role of cell interactions in fly glia migration and proliferation. Development 131:5127–5138.

Aigouy B, Lepelletier L, Giangrande A (2008) Glial chain migration requires pioneer cells. J Neurosci 28:11635–11641.

Arboleda-Estudillo Y, Krieg M, Stühmer J, Licata NA, Muller DJ, Heisenberg CP (2010) Movement directionality in collective migration of germ layer progenitors. Curr Biol 20:161–169.

Bardet PL, Kolahgar G, Mynett A, Miguel-Aliaga I, Briscoe J, Meier P, Vincent JP (2008) A fluorescent reporter of caspase activity for live imaging. Proc Natl Acad Sci U S A 105:13901–13905.

Boyen F, Eeckhaut V, Van Immerseel F, Pasmans F, Ducatelle R, Haesebrouck F (2009) Quorum sensing in veterinary pathogens: mechanisms, clinical importance and future perspectives. Vet Microbiol 135:187–195.

Friedl P, Gilmour D (2009) Collective cell migration in morphogenesis, regeneration and cancer. Nat Rev Mol Cell Biol 10:445–457.

Friedl P, Hegerfeldt Y, Tusch M (2004) Collective cell migration in morphogenesis and cancer. Int J Dev Biol 48:441–449.

Fristrom D, Wilcox M, Fristrom J (1993) The distribution of PS integrins, laminin A and F-actin during key stages in *Drosophila* wing development. Development 117:509–523.

Ghabrial AS, Krasnow MA (2006) Social interactions among epithelial cells during tracheal branching morphogenesis. Nature 441:746–749.

Giampieri S, Manning C, Hooper S, Jones L, Hill CS, Sahai E (2009) Localized and reversible TGFbeta signalling switches breast cancer cells from cohesive to single cell motility. Nat Cell Biol 11:1287–1296.

Giangrande A (1994) Glia in the fly wing are clonally related to epithelial cells and use the nerve as a pathway for migration. Development 120:523–534.

Hegerfeldt Y, Tusch M, Bröcker EB, Friedl P (2002) Collective cell movement in primary melanoma explants: plasticity of cell-cell interaction, beta1-integrin function, and migration strategies. Cancer Res 62:2125–2130.

Hellström M, Phng LK, Hofmann JJ, Wallgard E, Coultas L, Lindblom P, Alva J, Nilsson AK, Karlsson L, Gaiano N, Yoon K, Rossant J, Iruela-Arispe ML, Kalén M, Gerhardt H, Betsholtz C (2007) Dll4 signalling through Notch1 regulates formation of tip cells during angiogenesis. Nature 445:776–780.

Marín O, Valiente M, Ge X, Tsai LH (2010) Guiding neuronal cell migrations. Cold Spring Harb Perspect Biol 2:a001834.

Murray MJ, Saint R (2007) Photoactivatable GFP resolves *Drosophila* mesoderm migration behaviour. Development 134:3975–3983.

Soustelle L, Aigouy B, Asensio ML, Giangrande A (2008) UV laser mediated cell selective destruction by confocal microscopy. Neural Dev 3:11.

Valiente M, Marín O (2010) Neuronal migration mechanisms in development and disease. Curr Opin Neurobiol 20:68–78.

Vargas DA, Zaman MH (2011) Computational model for migration of a cell cluster in three-dimensional matrices. Ann Biomed Eng 39:2068–2079.